Applied Clay Science 190 (2020) 105565

Contents lists available at ScienceDirect

Applied Clay Science

journal homepage: www.elsevier.com/locate/clay

Research Paper

Nano-biocomposite films fabricated from cellulose fibers and halloysite nanotubes

Xiaohan Yang[a,b], Yangyang Zhang[b], Dingyuan Zheng[b], Jinquan Yue[b], Mingxian Liu[a,*]

[a] Department of Materials Science and Engineering, Jinan University, Guangzhou 510632, China
[b] College of Material Sciences and Engineering, Northeast Forestry University, Harbin 150040, China

ARTICLE INFO

Keywords:
Cellulose nanofiber
Halloysite
Composite
Morphology
Tensile strength

ABSTRACT

In this study, halloysite (Hal)/cellulose nanofiber (CNF) composite films were prepared using vacuum-filtering assembly method. Microstructures, chemical composition, crystal structures, thermal performances, mechanical properties, and light transmission properties of the composite films were characterized. The results showed that Hal was well uniformly dispersed in the composite films. The interactions between Hal and CNF endowed the formation of a robust network structure, and the surfaces of the composite films were rough by the addition of Hal. X-ray diffraction result showed the crystallinity of CNF declined by Hal, while the thermal stability of the composite films increased remarkably. The tensile strength of the composite films increased compared with pure CNF film, for example, the tensile strength and the elongation at break of the composite film with 3 Hal was 41.9 MPa and 11.7%, respectively. As the content of Hal in the composite film increased, the light transmittance of the composite film decreased, since the addition of Hal led to a growth in the haze of the composite films. The prepared high-performance Hal/CNF composite films show promising application in degradable food package.

1. Introduction

With the increasing population and consumables, non-renewable natural resources are consumed in large quantities. This has created a trend to explore sustainable raw materials from renewable sources. Cellulose is the most widely used bio-derived materials which has many superior properties such as good thermal and mechanical properties, good persistence, biocompatibility, and biodegradability (Darder et al., 2007; Sabir et al., 2009; Wang et al., 2016). The excellent properties of cellulose broaden its application in the textile industry, food science, composite reinforcement, bioengineering and other fields (Klemm et al., 2005; Pandey et al., 2010; Kalia et al., 2011). For instance, cellulose films made from cellulose can be used in display screens and solar cells due to their good transparency (Fang et al., 2014; Zhu et al., 2014). In addition, cellulose has also been widely used in other high-technique areas (Ragauskas et al., 2006; Jonoobi et al., 2010), especially in nanoscale forms such as cellulose nanocrystals (CNC) and cellulose nanofiber (CNF). For example, many researchers have studied CNF as a polymer reinforcement agent (Green et al., 2009; HPS et al., 2016).

Although cellulose transparent films have good transparency, there are still some drawbacks to be solved in practical applications (Siró and Plackett, 2010; Lavoine et al., 2012). One of challenges is that how to control the haze of the cellulose transparent film. Haze refers to the amount of light that is scattered by a wide angle (Krogman et al., 2005). Two kinds of haze are often used in materials, one is reflective haze and the other is transmissive haze. The former depends to a great extent on the reflection of a surface, while the other one is related to the refraction and scattering of light by the film (Ulrich and Martin, 1971; Bousquet et al., 1981). Films used in automotive sunroofs require higher haze to reduce direct light exposure and reduce visual fatigue. In recent years, more and more researchers have tried to control the haze of materials by addition of nanoscale particles (Krogman et al., 2005). However, when the size of the particles reaches the nanometer scale, the agglomeration of the particles makes it difficult to uniformly disperse in the medium (Perrut et al., 2005; Xia et al., 2010), which has a negative influence on transparency and mechanical properties.

Halloysite (Hal), with a hollow tubular structure, is mainly composed of aluminosilicate with molecular formula of $Al_2O_3.2SiO_2.2H_2O$ (Lvov et al., 2008; Kamble et al., 2012). Hal usually displays a tubular morphology, so it is generally known as halloysite nanotubes. Hal, as natural one-dimensional clay minerals, exhibits predominantly hollow tubular nanostructures and high aspect ratios (Liu et al., 2014, 2019). Hal with a 15 nm in lumen, 50 nm external in diameter, and length of 200–2000 nm has been developed as an encapsulation system for loading (Yuan et al., 2015; Garcia-Garcia et al., 2018; Kurczewska et al.,

* Corresponding author.
E-mail address: liumx@jnu.edu.cn (M. Liu).

https://doi.org/10.1016/j.clay.2020.105565
Received 15 October 2019; Received in revised form 11 March 2020; Accepted 12 March 2020

2018), storage, and controlled release of anticorrosion agents and biocides (Guimaraes et al., 2010; Abdullayev and Lvov, 2013). Hal exhibits superior mechanical strength and modulus (Liu et al., 2012), so it is widely used to enhance the mechanical properties of polymers (Shchukin et al., 2005; Lvov et al., 2016). Based on the different chemical properties of Hal between the outer surface and cylindrical lumen, natural Hal can carry many chemicals and biologically active substances drugs on their functionalized surfaces (Liu et al., 2013; Lvov and Abdullayev, 2013). Hal shows great potential in different areas (Du et al., 2010), such as anti-corrosion coatings, catalyst for hydrogen production and storage, pharmaceutical excipients, biomedicine (Vergaro et al., 2010; Lvov et al., 2016), cosmetics, food packaging materials, water treatment (Fan et al., 2019). Globally, the production of Hal is more than 50,000 tons per year, which is comparable to annual carbon fiber production (40,000 t/y).

Specially, Hal with unique tubular structures, as rigid inorganic materials (Liu et al., 2009), is ideal materials for the preparation of polymer composites (Du et al., 2010). Compared with other nanoparticles such as fumed silica, montmorillonite, and carbon nanotubes (Liu et al., 2009; Prashantha et al., 2011), Hal is more easily dispersed in the polymer matrix by a certain shear force. In fact, morphological studies of many Hal/polymer composites have shown a single tube of dispersed Hal in the matrix. And chemically, Hal has a relatively low hydroxyl density on the outer surface compared to fumed silica and other layered silicates such as montmorillonite (Liu et al., 2008; Prashantha et al., 2011). In addition, Hal is environmentally friendly, non-toxic and compatible for a range of microorganisms, cell cultures and animal models. Besides, clay nanomaterials have additional economic benefits compared to other nanofillers such as carbon nanotubes. In a word, Hal is green and promising reinforcement material for polymers (Prashantha et al., 2011). Moreover, it is reported that the bionanocomposite films with good properties have been prepared from regenerated cellulose and Hal with ionic liquid (Soheilmoghaddam and Wahit, 2013). Previously, Hal/cellulose composite hydrogels were prepared by dissolving the cellulose in alkali/urea systems for curcumin delivery (Huang et al., 2017).

In this study, the structural characteristics of the natural nanotubes of Hal were firstly characterized. The Hal/CNF composite films were prepared by adding different concentrations of Hal to explore their effect on the properties of the composite film. By vacuum-filtering assembly method, the free-standing composites films composed with CNF and Hal were obtained. The properties changes of the cellulose film are correlated to the composition of the composites and the interactions between the components.

2. Experimental

2.1. Materials

Poplar wood powder (60–80 meshes) was acquired by Maoershan Forest Farm, China. Hal was obtained from Shijiazhuang Lingshou County Mineral Processing Factory, China. Concentrated hydrochloric acid was purchased from Xiqiao Science Co., Ltd., China. Hexametaphosphate was supplied from Tianjin Komiou Chemical Reagent Co., Ltd., China. Other chemicals of analytical grade were purchased from Tianjin Fuyu Fine Chemical Co., Ltd.

2.2. CNF preparation experimental steps

2.2.1. Chemical pretreatment

In this study, chemical pretreatment combined with mechanical separation was used to prepare CNF. Firstly, the impurity components such as extracts were removed andthe poplar wood powder of 60–80 meshes size was obtained. Next, a vinyl alcohol solution with a volume ratio of 2:1 and a volume of 300 mL was prepared, then the wrapped poplar wood powder was put into a Soxhlet extractor and kept at constant temperature water bath at a temperature of 90 °C. The extraction was carried out for 6 h. Finally, the wood powder was filled into a fume hood for air drying, and the phenyl alcohol was completely evaporated (Pérez et al., 2002). The removal of lignin components and hemicellulose component was carried out according to the references (Ramiah, 1970; Hosoya et al., 2007).

2.2.2. Increasing the dispersibility between the filaments

A certain concentration of hydrochloric acid was added to the purified cellulose, and the beaker was continuously shaken to allow the purified cellulose to be dispersed in hydrochloric acid. Then, the beaker was sealed with a sealed bag and placed it in a constant temperature water bath at a certain temperature with stirring. After the reaction, suction filtration was carried out using a Buchner funnel, and the purified cellulose was repeatedly washed with distilled water until the solution became neutral.

2.2.3. Mechanical treatment

High-intensity sonication was carried out to perform mechanical treatment. First, the concentration of the cellulose solution obtained was measured by a solvent solution method, and the obtained cellulose was diluted with distilled water to prepare a cellulose solution for a desired concentration of 0.8 wt%. The prepared cellulose was placed in an ultrasonic cell disruptor, and the output power was set as 1000 W, and ultrasonic treatment was performed for 30 mins while maintaining the ice water bath environment. Eventually, CNF with molar mass of 97, 200–129, 000 $g \cdot mol^{-1}$ were obtained.

2.3. Preparation of Hal dispersion

The experimental product Hal 0.1 g was dispersed in 100 mL of distilled water, placed in an ultrasonic cleaner for 40 mins, and shaken once every 10 mins during ultrasonication. After 10 mins, a small amount of NaOH (NaOH solid) was added, then the pH of the solution was slowly adjusted to 8. Then, 0.0003 g of sodium hexametaphosphate was added to the above solution, and the ultrasonication was continued for 40 mins, shaking once every 10 mins. The addition of sodium hexametaphosphate was to prevent the agglomeration of Hal. In this way, Hal can be uniformly dispersed (Churchman and Gilkes, 1989), spread on the surface of the CNF film, and the surface of the composite film was evenly continuous.

2.4. Preparation of Hal/CNF composite films

The process of preparing Hal/CNF composite films was shown in Fig. 1. Firstly, 4 mL of CNF solution was collected and then filtered the solution under the glass sand core funnel to obtain CNF film. To obtain the composite films with different concentrations of Hal, 0 mL, 0.5 mL, 1 mL, 1.5 mL and 2.0 mL of Hal solution were separately added to the CNF film, and then filter again. The obtained Hal/CNF composite film samples were labeled as 0 Hal, 1 Hal, 2 Hal, 3 Hal and 4 Hal, corresponding the mass ratio of Hal in the composites of 0%, 1.56%, 3.12%, 4.69%, 6.25%, respectively. Additionally, the diameter of the prepared composite film was 42 mm. Then, the film was pressed using a hot press at 100 °C at a pressure of 2 MPa and dried by hot pressing for 8 mins.

2.5. Characterization of composite film

2.5.1. 3D morphology

The surface morphology and roughness of the pure film and the composite film were observed by a 3D optical profilometer (UP-DUAL MODE, Rtec Engineering Ltd., USA) with magnification of 500 X (Wu et al., 2019). The 3D profile of the coating surface was inspected with a 3D optical profiler with a test area of 0.5 mm × 0.5 mm (CF mode). The line profiles were obtained by analyzing the 3D topography by Gwyddion analysis software.

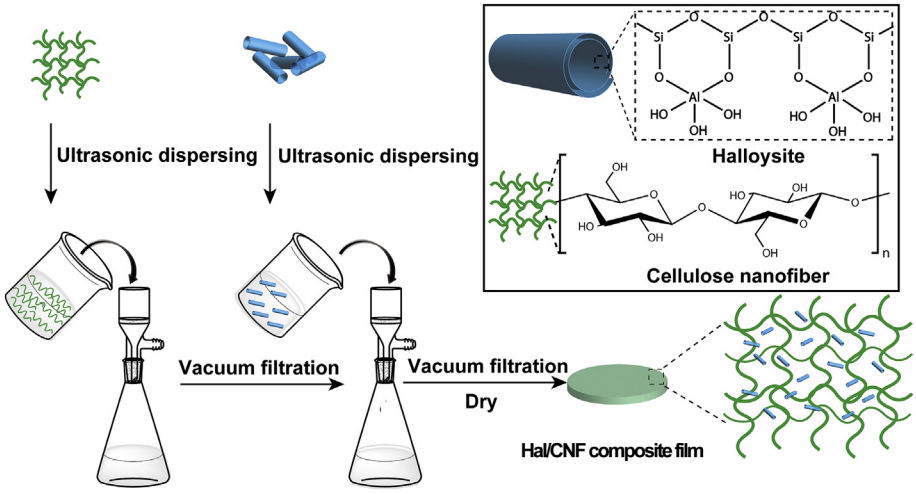

Fig. 1. Schematic diagram of the preparation of Hal/CNF composite films.

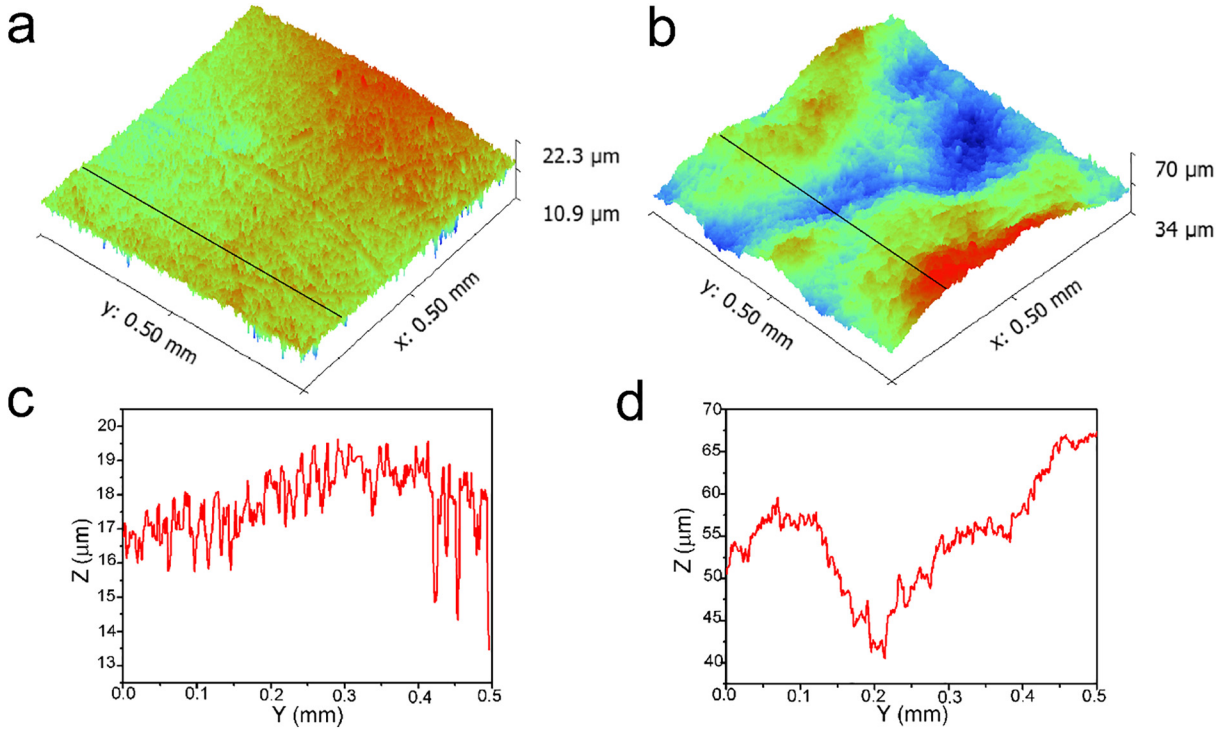

Fig. 2. 3D topography and roughness curve of the pure cellulose film and the composite film with 4 Hal: (a) topographic images of pure cellulose film, (b) topographic images of the composite film, (c) height profiles of pure cellulose film and (d) height profiles of composite film with 4 Hal.

2.5.2. Electron microscopy analysis

A Quanta200 scanning electron microscope (SEM) was used for the detection of the cross-section of the Hal/CNF composite film and the spreading of Hal on the surface of the CNF film. The test condition was set to a high vacuum mode and the operating voltage was set to 15 kV. The morphology of Hal was observed by TEM (JEM-2100F, JEOL Ltd., Japan) under an accelerating voltage of 100 kV. The concentration of Hal dispersion for TEM test was 0.05 wt%.

2.5.3. XPS elemental analysis

In order to check the elemental composition and chemical bonding state of Hal and CNF, the composition and chemical bonding state of the surface elements of the sample were analyzed by a K-Alpha type X-ray photoelectron spectrometer (ESCALAB250Xi, Thermo Fisher Scientific Ltd., USA). The operating conditions were set to an X-ray beam current of 6 mA with a scan step of 0.1 eV and an energy resolution of 0.5 eV.

2.5.4. Fourier transform infrared spectrum analysis (FT-IR)

To check the chemical combination of Hal and CNF, a Magna-IR 560E.S·P type Fourier infrared spectrometer (FT-IR) was used at scan range to 400 cm^{-1}–4000 cm^{-1} and tested with ATR accessories.

2.5.5. X-ray diffraction analysis

D/MAX2200 X-ray diffractometer (XRD) with an Ni filter and Cu Kα radiation manufactured by Nippon Science and Technology Co., Ltd. was used to detect the crystal structure in the 2θ range of 5 to 70°. The scan rate was 5°(2θ)/min. The current and the voltage were 30 mA and 40 kV, respectively. The wavelength of the ray was 0.154 nm, and the crystallinity was calculated according to the Segal method.

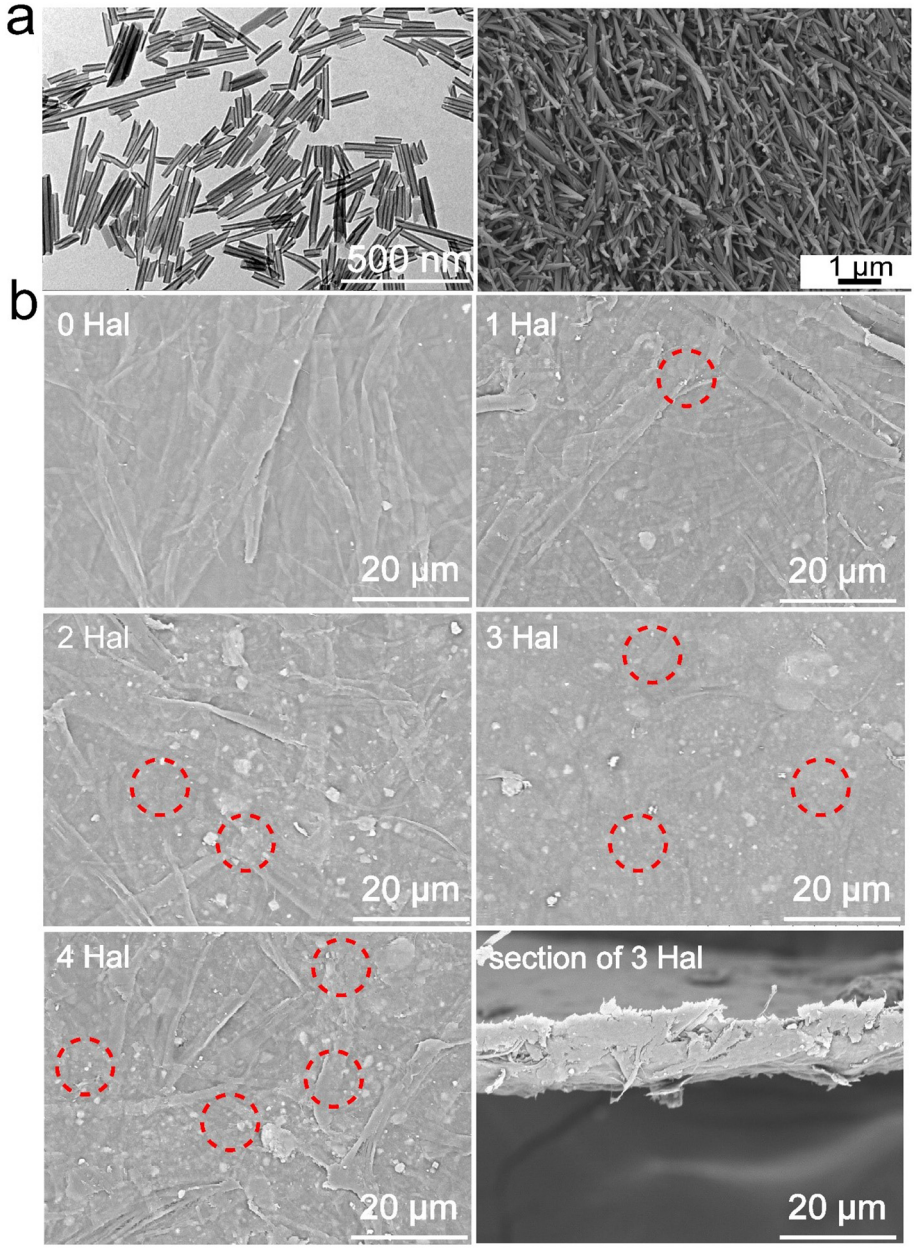

Fig. 3. Microscope images: (a) TEM and SEM of Hal; (b) SEM images of 0 Hal, 1 Hal, 2 Hal, 3 Hal, 4 Hal and the section of 3 Hal.

2.5.6. Thermal stability analysis

The thermal stability of the composite film was tested using a Pyris6 Thermogravimetric Analyzer (TG) from Perkin-Elmer, USA. The sample was gradually heated from room temperature at a heating rate of 10 °C/min in a N_2 atmosphere (40 cm^3/min) until the sample was completely pyrolyzed at 700 °C.

2.5.7. Tensile performance test

In order to test the mechanical properties of the Hal/CNF composite film, the mechanical properties of the specimens were tested at room temperature using a US Instron 5569 model. The tensile rate was set as 10 mm/min. The length, width and thickness of the sample for tensile property determination were 35, 5, and 0.03 mm, respectively.

2.5.8. Analysis of light transmission performance

In order to examine the light transmission properties of the Hal/CNF composite film, the transmittance of the film was measured using a UH4150 Spectrophotometer with Integrating Sphere equipped with a 60 mm diameter integrating sphere. The scanning speed was set to 300 nm/min and the wavelength range was 400 to 750 nm. The sampling interval was set to 0.5 nm and the spectral bandwidth was 6 nm. The test was conducted at a temperature of 25 °C and a sensitivity of 100%. To ensure the accuracy of the test, each sample was tested for 3 times.

3. Results and discussion

3.1. 3D topography morphology

The surface property of pure CNF film and the composite film with 4 Hal were firstly observed by a 3D optical profilometer within 0.5 × 0.5 mm area (Fig. 2), and the pattern heights were given by the difference between tops and valleys in the profile curves. The height (pattern thickness) of composite film with 4 Hal was 33.01 ± 2.98 μm, which was 28.4 μm higher than that of pure cellulose film (4.61 ± 0.46 μm). This suggested that the height of the composite film

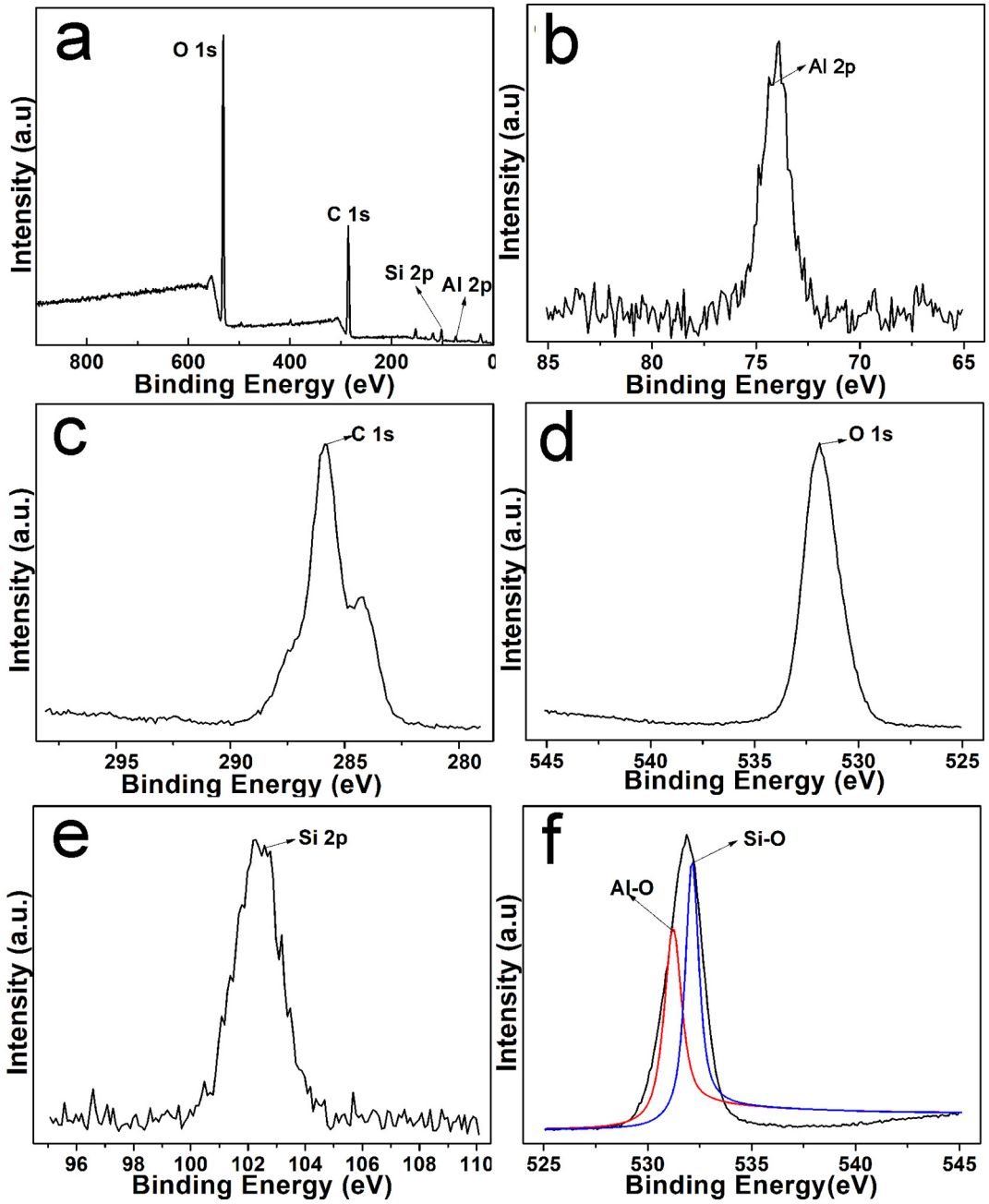

Fig. 4. XPS spectra of Hal/CNF composite films of 3 Hal.

was much greater than that of the pure cellulose film. Therefore, the surface was much rougher than that of pure film after adding 4 Hal. The increased surface roughness of the composite film was caused by the presence of micro spacing brought by different size of cellulose fiber and Hal. Similar result was also noted in other Hal coated polymer surfaces, such as Hal treated 3D printing polylatic acid pattern surface was much rougher than that untreated surface (Wu et al., 2019). It should be pointed out that no single Hal can be identified since the 3D optical profilometer has low resolution compared atomic force microscopy.

3.2. SEM analysis

The morphology of Hal was given in Fig. 3a. Hal showed typical tubular morphology with empty lumen and high aspect ratio. However, the length had wide distribution from 200 to 1500 nm. As demonstrated in Fig. 3b, Hal was uniformly dispersed on the film, but it can be found that some agglomeration occurred. Although sodium hexametaphosphate was added, most of the tubes were uniformly dispersed on the film with partial aggregations. This may be caused by the drying-induced aggregation during the preparation of the composite film (Liu et al., 2007). Even by high-strength mechanical stirring, the agglomerated particles were sometimes difficult to disperse. In order to uniformly disperse the nanoparticles, the surface of the particles needed to be chemically or electrostatically modified (Grzelczak et al., 2010). However, the Hal in this experiment showed satisfactory dispersibility in the CNF film matrix, which was mainly caused by the characteristics of the surface charge distribution of Hal. The siloxane groups on the surface of the Hal made them to be negatively charged (Song et al., 2020), which produced a strong inter-tube repulsive force, which in turn allowed the Hal to be uniformly dispersed in the CNF. Hal was not only distributed on the surface of the film, but also some had entered

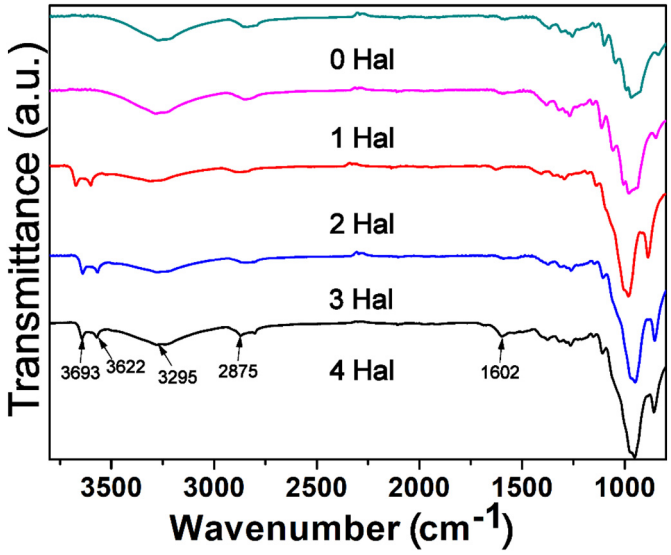

Fig. 5. FT-IR spectra of Hal/CNF composite films at different Hal concentrations.

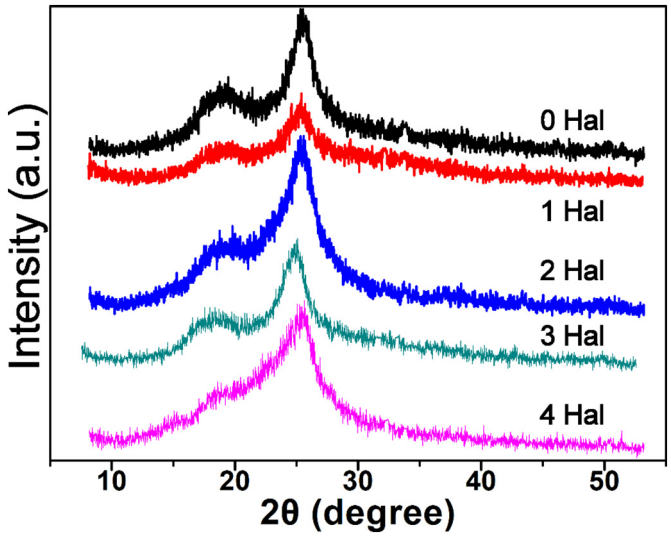

Fig. 6. XRD spectra of Hal/CNF composite films at different Hal concentrations.

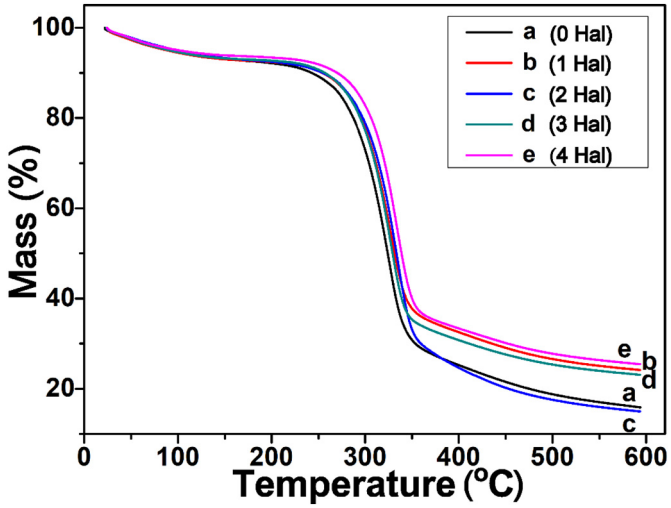

Fig. 7. Thermodynamic properties of Hal/CNF composite films at different concentrations of Hal.

the CNF network and intertwined with CNF (Fig. 3b). Besides, according to the results of FT-IR below, there were hydrogen bond interactions between the Hal and CNF.

3.3. The chemical composition

Fig. 4a was a full-spectrum XPS scan of a composite film with 3 Hal. The absorption bands of Al 2p, C 1s, O 1s and Si 2p element were at 73.88, 285.86, 525.18, and 102.18 eV, respectively (Fig. 4b-e). The contents of C element and O element were higher, but the contents of Al element and Si element were less. The content of C element was 48.34%, while Al, O, and Si elements had ratio of 3.87%, 43.40%, and 4.39%, respectively. According to the Hal structure ($Al_2O_3{\cdot}2SiO_2{\cdot}4H_2O$), there were mainly Al and Si elements, and the contents were 45.8% for SiO_2 and 37.3% for Al_2O_3. The hollow-shaped Hal has a skeleton composed of an O element, a Si element and an Al element (Pierchala et al., 2018), and the inner surface and the outer surface there are rich in hydroxyl groups (Deng et al., 2019). This structural feature indicated that there was more O element exposed on the inner and outer surfaces, but the Si and Al elements became less exposed. Therefore, in the full-spectrum scan, the content of O element was higher, but the contents of Si element and Al element were less. According to the band fitting result of the O1s line, the different sub-bands of O1s can be obtained (Fig. 4f). The binding energy of the A-sub-band was 531.1 eV corresponding to Al—O, and the binding energy of the B-band was 532.5 eV corresponding to Si—O. The presence of both Si and Al further demonstrated the presence of Hal on the surfaces of the composite film.

3.4. FT-IR

In order to study whether the composite cellulose film produced chemical changes, the material was subject to FT-IR test analysis (Fig. 5). In this experiment, as the content of Hal in the Hal/CNF composite film increased, the thickness of the CNF film was slightly increased. The absorption band at 3295 cm^{-1} represented the stretching vibration of –OH of cellulose (Ledoux and White, 1964), while the absorption band at 2875 cm^{-1} was characterized by the $–CH_2$, C—H stretching vibration. The absorption band at 1602 cm^{-1} indicated the stretching vibration of the H-O-H group in the water absorbed by the carbohydrate. The characteristic bands of hydroxyl group at 3693 and 3622 cm^{-1} of Hal can be found in the composite with 2 Hal loading in Fig. 5. Additionally, with Hal content increasing, the strength of the characteristic bands became larger. In contrast, the characteristic bands of –OH in cellulose was slightly decreased, which showed the existence of hydrogen bonds between CNF and Hal. Besides, there were hydrogen bonds present between CNF and Hal in previous work (Huang et al., 2017). It can be found from the FT-IR spectrum that the main components of the Hal/CNF composite film with different Hal content were cellulose and a small amount of hemicellulose, which indicated that the structure and chemical composition of cellulose molecules were not changed during the preparation of the CNF film. Since there was hydrogen bonding interaction between CNF and Hal, Hal was expected to be uniformly dispersed in the composite film from surface to bottom. However, according to the SEM characterization results, Hal was not only uniformly dispersed on the surface of the CNF film, but also partially entered the different positions inside the CNF film.

3.5. The crystal structure and crystallinity

The XRD pattern for different samples was then investigated (Fig. 6). The reflections of the Hal/CNF composite film at different Hal concentrations did not show a significant difference with pure cellulose. The addition of Hal did not possess a significant effect on the crystallinity of the CNF especially at low Hal content according to the Segal

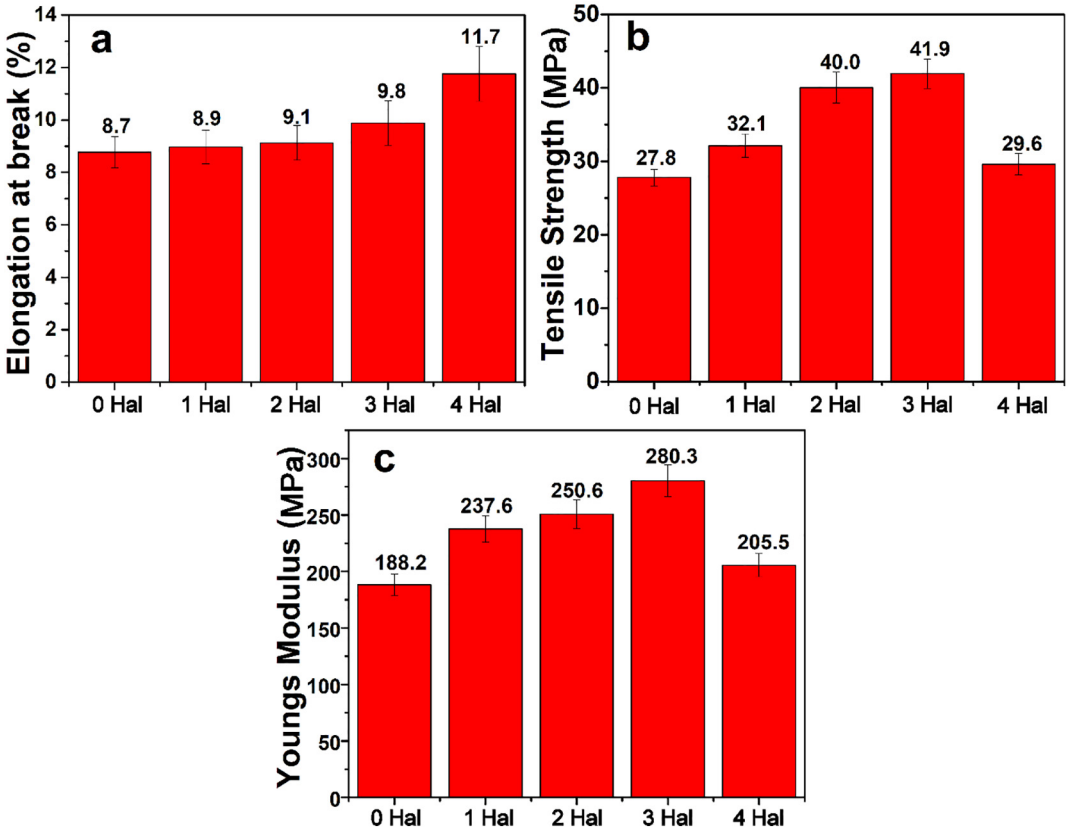

Fig. 8. Mechanical performance diagram of Hal/CNF composite film, (a) Elongation at break (b) Tensile strength change (c) Young's modulus.

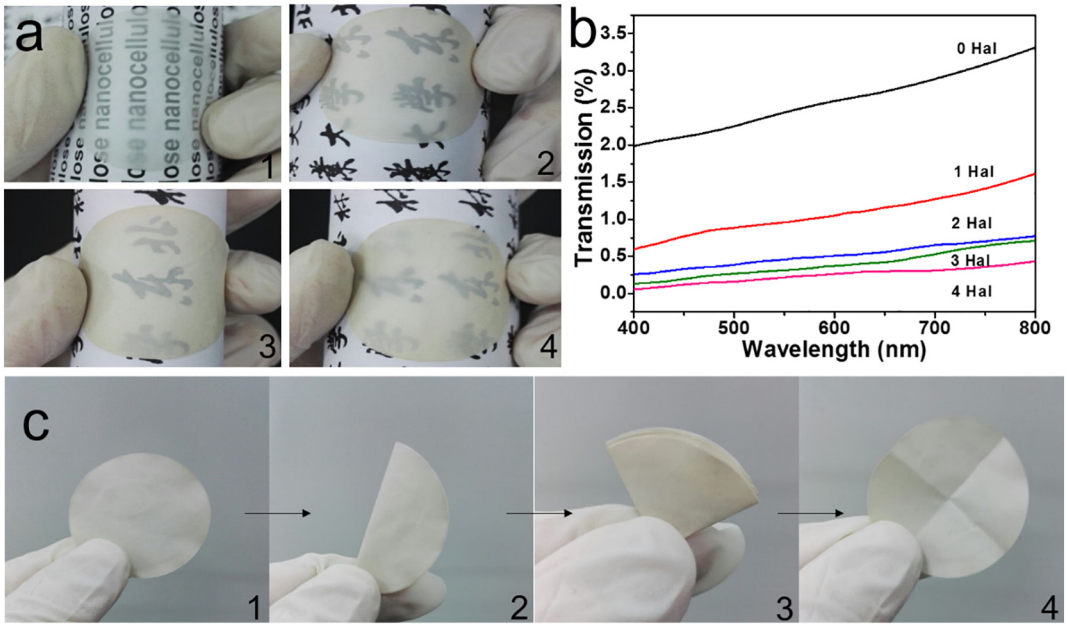

Fig. 9. The flexibility and light transmission performance of Hal/CNF composite films: (a) different light transmittance in the same color environment; (b) light transmission performance and (c) composite film flexibility under 4 Hal.

method (French and Cintrón, 2013). At the same time, it can be observed that CNF still retained two typical natural cellulose I type structure diffraction characteristic reflections (2θ = 18.52°, 2θ = 22.56°). The position of the characteristic reflections of cellulose slightly shifted compared to pure cellulose, which indicated that the crystalline structure of the CNF had not been altered after chemical pretreatment and high-pressure homogenization, which guaranteed CNF with high crystallinity contributed to the improvement of the mechanical properties and thermal stability of the polymer composite film. No characterized reflections of Hal can be identified for the patterns of the composites, which can be understood by the small amount of Hal in the composites.

3.6. Thermal stability analysis

The TG analysis of the pure CNF film and the composite films with different contents of Hal in a nitrogen atmosphere were conducted (Fig. 7). The temperature at which the composite films initially degraded was 220 °C, which was same as the TG curve of pure CNF film. This indicated that sonication and homogenization did not significantly reduce the thermal stability of the CNF. From the curve b-e in Fig. 7, the increase in Hal loading had a certain effect on the thermal stability of composites. The thermal stability of Hal/CNF composite films was enhanced to some extent by adding Hal as it indicated in the 4 Hal group. Significantly, when the mass loss was 50%, the T_{50} value of 4 Hal group (340 °C) was increased by 16 °C, while the T_{50} of the pure CNF film was 324 °C. Furthermore, from the data in the Fig. 7, the residue of the pure CNF was less than that of the other three groups at 600 °C, especially compared to the 4 Hal group. The reason for the enhancement may be that the thermal stability of the composite film increased due to the introduction of the nanoparticles (Garcia-Garcia et al., 2018). Therefore, the improvement in thermal stability of Hal/CNF composites was attributed to the addition of thermal-stable inorganic Hal.

3.7. Mechanical performance analysis

The effect of Hal content on the elongation at break of Hal/CNF composite films was studied (Fig. 8a). The elongation at break of the Hal/CNF nanocomposite film was improved compared to the pure CNF film. With the increase of Hal content, the elongation at break of the film increased from 8.7% of 0 Hal to 11.7% of 3 Hal. From Fig. 8b, the tensile strength of the Hal/CNF composite film was greater than that of the pure CNF film. Additionally, the tensile strength of the Hal/CNF composite film containing 3 Hal displayed a significant increase of 50.7%, which was possibly due to various factors such as good dispersion of Hal in CNF and interfacial interactions between Hal/CNF. However, according to Fig. 8b, as the Hal content further grew up, the tensile strength fell down. This may be that higher concentrations of Hal may have some aggregation. Fig. 8c represents that the Young's modulus of Hal/CNF films was affected by the concentration of Hal. Besides, the Young's modulus of the Hal/CNF composite film increased linearly until the concentration of 3 Hal was reached. Moreover, the Young's modulus of 3 Hal was enhanced by 48.9% compared with 0 Hal. However, as the Hal content further increased to 4 Hal, the Young's modulus decreased. Significant improvement in Young's modulus of Hal/CNF films may be related to the reinforcement effect of the tubular nanoparticles. It was also related to the well dispersion of Hal in composite film.

3.8. Flexibility and light transmission performance analysis

All the films prepared were transparent without any black spots (Fig. 9a). As the Hal content increased, the light transmission of the Hal/CNF composite film gradually decreased. Fig. 9b demonstrates the optical properties of the Hal/CNF composite film. The optical properties of CNF films demonstrated these films were suitable for application in the field of green electronics or food packaging. With the less light transmittance, the composite films can keep the food away from the light, which was beneficial to the food preservation. According to the Fig. 9b, as more Hal were added, the light transmittance gradually decreased. For example, the transmittance of pure CNF film at 800 nm was about 3.4%, while the values of Hal/CNF composite film were reduced to 1.5%, 0.75%, 0.5% and 0.3% corresponding to 1 Hal, 2 Hal, 3 Hal and 4 Hal, respectively. The reason for the low transmittance of pure CNF may be explained by the slightly higher concentration of CNF in this experiment. As the diameter of CNF increased, the amount of light scattering went up significantly, leading to a decrease in light transmittance. In addition, the cause for the decline in light transmittance of the Hal/CNF composite film may be that the distribution of Hal in the CNF matrix had a significant effect on transparency. The composite film had good flexibility by releasing it after two folds (Fig. 9c). Besides, when immersing in water for 14 days, the composite films did not break down. Since they have resistance to water, they show potentials in packaging materials.

4. Conclusion

Nano-biocomposite film composed with CNF and Hal was successfully prepared by vacuum filtration. The results showed Hal had good dispersibility in CNF film. Furthermore, the surface of composite film was much rougher than that of pure film after adding 4 Hal. Hydrogen bond interaction between CNF and Hal was detected by FT-IR analysis. The enhancement in thermal stability of Hal/CNF composites was attributed to the addition of thermal-stable inorganic Hal. The tensile strength of the composite films remarkable increased compared with pure CNF film. With the increasing content of Hal in the composite film, the light transmittance of the composite film went down gradually. Additionally, the composite film had good flexibility without fracture by folding. All the results suggested that composite films with controllable haze and mechanical properties showed potentials in the degradable food package.

Declaration of Competing Interest

The authors declare that they have no known competing financial interests or personal relationships that could have appeared to influence the work reported in this paper.

Acknowledgements

This work was financially supported by the National Natural Science Foundation of China (51473069 and 51502113), Guangdong Basic and Applied Basic Research Foundation (2019A1515011509), and the Fundamental Research Funds for the Central Universities (21619102).

References

Abdullayev, E., Lvov, Y., 2013. Halloysite clay nanotubes as a ceramic “skeleton” for functional biopolymer composites with sustained drug release. J. Mater. Chem. B 1, 2894–2903.
Bousquet, P., Flory, F., Roche, P., 1981. Scattering from multilayer thin films: theory and experiment. J. Opt. Soc. Am. 71, 1115–1123.
Churchman, G., Gilkes, R., 1989. Recognition of intermediates in the possible transformation of halloysite to kaolinite in weathering profiles. Clay Miner. 24, 579–590.
Darder, M., Aranda, P., Ruiz-Hitzky, E., 2007. Bionanocomposites: a new concept of ecological, bioinspired, and functional hybrid materials. Adv. Mater. 19, 1309–1319.
Deng, L., Yuan, P., Liu, D., Du, P., Zhou, J., Wei, Y., Song, Y., Liu, Y., 2019. Effects of calcination and acid treatment on improving benzene adsorption performance of halloysite. Appl. Clay Sci. 181, 105240.
Du, M., Guo, B., Jia, D., 2010. Newly emerging applications of halloysite nanotubes: a review. Polym. Int. 59, 574–582.
Fan, W., Pickett, K., Panchal, A., Liu, M., Lvov, Y.M., 2019. Super-hydrophobic polyurethane foam coated with polysiloxane-modified clay nanotubes for efficient and recyclable oil absorption. ACS Appl. Mater. Interfaces 11, 25445–25456.
Fang, Z., Zhu, H., Yuan, Y., Ha, D., Zhu, S., Preston, C., Chen, Q., Li, Y., Han, X., Lee, S., 2014. Novel nanostructured paper with ultrahigh transparency and ultrahigh haze for solar cells. Nano Lett. 14, 765–773.
French, A.D., Cintrón, M.S., 2013. Cellulose polymorphy, crystallite size, and the Segal crystallinity index. Cellulose 20, 583–588.
Garcia-Garcia, D., Garcia-Sanoguera, D., Fombuena, V., Lopez-Martinez, J., Balart, R., 2018. Improvement of mechanical and thermal properties of poly (3-hydroxybutyrate)(PHB) blends with surface-modified halloysite nanotubes (HNT). Appl. Clay Sci. 162, 487–498.
Green, K.J., Dean, D.R., Vaidya, U.K., Nyairo, E., 2009. Multiscale fiber reinforced composites based on a carbon nanofiber/epoxy nanophased polymer matrix: synthesis, mechanical, and thermomechanical behavior. Composites Part A 40, 1470–1475.
Grzelczak, M., Vermant, J., Furst, E.M., Liz-Marzan, L.M., 2010. Directed self-assembly of nanoparticles. ACS Nano 4, 3591–3605.
Guimaraes, L., Enyashin, A.N., Seifert, G., Duarte, H.A., 2010. Structural, electronic, and mechanical properties of single-walled halloysite nanotube models. J. Phys. Chem. C 114, 11358–11363.
Hosoya, T., Kawamoto, H., Saka, S., 2007. Cellulose–hemicellulose and cellulose–lignin

interactions in wood pyrolysis at gasification temperature. J. Anal. Appl. Pyrolysis 80, 118–125.
HPS, A.K., Saurabh, C.K., Adnan, A., Fazita, M.N., Syakir, M., Davoudpour, Y., Rafatullah, M., Abdullah, C., Haafiz, M., Dungani, R., 2016. A review on chitosan-cellulose blends and nanocellulose reinforced chitosan biocomposites: properties and their applications. Carbohydr. Polym. 150, 216–226.
Huang, B., Liu, M., Zhou, C., 2017. Cellulose-halloysite nanotube composite hydrogels for curcumin delivery. Cellulose 24, 2861–2875.
Jonoobi, M., Harun, J., Mathew, A.P., Oksman, K., 2010. Mechanical properties of cellulose nanofiber (CNF) reinforced polylactic acid (PLA) prepared by twin screw extrusion. Compos. Sci. Technol. 70, 1742–1747.
Kalia, S., Dufresne, A., Cherian, B.M., Kaith, B., Avérous, L., Njuguna, J., Nassiopoulos, E., 2011. Cellulose-based bio-and nanocomposites: a review. Int. J. Polym. Sci. 2011, 1–35.
Kamble, R., Ghag, M., Gaikawad, S., Panda, B.K., 2012. Halloysite nanotubes and applications: a review. J. Adv. Sci. Res. 3, 25–29.
Klemm, D., Heublein, B., Fink, H.P., Bohn, A., 2005. Cellulose: fascinating biopolymer and sustainable raw material. Angew. Chem. Int. Ed. 44, 3358–3393.
Krogman, K.C., Druffel, T., Sunkara, M.K., 2005. Anti-reflective optical coatings incorporating nanoparticles. Nanotechnology 16, S338.
Kurczewska, J., Cegłowski, M., Messyasz, B., Schroeder, G., 2018. Dendrimer-functionalized halloysite nanotubes for effective drug delivery. Appl. Clay Sci. 153, 134–143.
Lavoine, N., Desloges, I., Dufresne, A., Bras, J., 2012. Microfibrillated cellulose–its barrier properties and applications in cellulosic materials: a review. Carbohydr. Polym. 90, 735–764.
Ledoux, R.L., White, J.L., 1964. Infrared study of the OH groups in expanded kaolinite. Science 143, 244–246.
Liu, M., Guo, B., Du, M., Jia, D., 2007. Drying induced aggregation of halloysite nanotubes in polyvinyl alcohol/halloysite nanotubes solution and its effect on properties of composite film. Appl. Phys. A Mater. Sci. Process. 88, 391–395.
Liu, M., Guo, B., Zou, Q., Du, M., Jia, D., 2008. Interactions between halloysite nanotubes and 2, 5-bis (2-benzoxazolyl) thiophene and their effects on reinforcement of polypropylene/halloysite nanocomposites. Nanotechnology 19, 205709.
Liu, M., Guo, B., Du, M., Chen, F., Jia, D., 2009. Halloysite nanotubes as a novel β-nucleating agent for isotactic polypropylene. Polymer 50, 3022–3030.
Liu, M., Zhang, Y., Wu, C., Xiong, S., Zhou, C., 2012. Chitosan/halloysite nanotubes bionanocomposites: structure, mechanical properties and biocompatibility. Int. J. Biol. Macromol. 51, 566–575.
Liu, M., Wu, C., Jiao, Y., Xiong, S., Zhou, C., 2013. Chitosan–halloysite nanotubes nanocomposite scaffolds for tissue engineering. J. Mater. Chem. B 1, 2078–2089.
Liu, M., Jia, Z., Jia, D., Zhou, C., 2014. Recent advance in research on halloysite nanotubes-polymer nanocomposite. Prog. Polym. Sci. 39, 1498–1525.
Liu, M., Cao, X., Liu, H., Yang, X., Zhou, C., 2019. Halloysite-based polymer nanocomposites. In: Wang, A., Wang, W. (Eds.), Micro and Nano Technologies, Nanomaterials from Clay Minerals. Elsevier, pp. 589–626.
Lvov, Y., Abdullayev, E., 2013. Functional polymer–clay nanotube composites with sustained release of chemical agents. Prog. Polym. Sci. 38, 1690–1719.
Lvov, Y.M., Shchukin, D.G., Mohwald, H., Price, R.R., 2008. Halloysite clay nanotubes for controlled release of protective agents. ACS Nano 2, 814–820.
Lvov, Y., Wang, W., Zhang, L., Fakhrullin, R., 2016. Halloysite clay nanotubes for loading and sustained release of functional compounds. Adv. Mater. 28, 1227–1250.
Pandey, J.K., Ahn, S., Lee, C.S., Mohanty, A.K., Misra, M., 2010. Recent advances in the application of natural fiber based composites. Macromol. Mater. Eng. 295, 975–989.
Pérez, J., Munoz-Dorado, J., De la Rubia, T., Martinez, J., 2002. Biodegradation and biological treatments of cellulose, hemicellulose and lignin: an overview. Int. Microbiol. 5, 53–63.
Perrut, M., Jung, J., Leboeuf, F., 2005. Enhancement of dissolution rate of poorly-soluble active ingredients by supercritical fluid processes: part I: micronization of neat particles. Int. J. Pharm. 288, 3–10.
Pierchala, M.K., Makaremi, M., Tan, H.L., Pushpamalar, J., Muniyandy, S., Solouk, A., Lee, S.M., Pasbakhsh, P., 2018. Nanotubes in nanofibers: antibacterial multilayered polylactic acid/halloysite/gentamicin membranes for bone regeneration application. Appl. Clay Sci. 160, 95–105.
Prashantha, K., Lacrampe, M.-F., Krawczak, P., 2011. Processing and characterization of halloysite nanotubes filled polypropylene nanocomposites based on a masterbatch route: effect of halloysites treatment on structural and mechanical properties. Express Polym Lett 5, 295–307.
Ragauskas, A.J., Williams, C.K., Davison, B.H., Britovsek, G., Cairney, J., Eckert, C.A., Frederick, W.J., Hallett, J.P., Leak, D.J., Liotta, C.L., 2006. The path forward for biofuels and biomaterials. Science 311, 484–489.
Ramiah, M., 1970. Thermogravimetric and differential thermal analysis of cellulose, hemicellulose, and lignin. J. Appl. Polym. Sci. 14, 1323–1337.
Sabir, M.I., Xu, X., Li, L., 2009. A review on biodegradable polymeric materials for bone tissue engineering applications. J. Mater. Sci. 44, 5713–5724.
Shchukin, D.G., Sukhorukov, G.B., Price, R.R., Lvov, Y.M., 2005. Halloysite nanotubes as biomimetic nanoreactors. Small 1, 510–513.
Siró, I., Plackett, D., 2010. Microfibrillated cellulose and new nanocomposite materials: a review. Cellulose 17, 459–494.
Soheilmoghaddam, M., Wahit, M.U., 2013. Development of regenerated cellulose/halloysite nanotube bionanocomposite films with ionic liquid. Int. J. Biol. Macromol. 58, 133–139.
Song, Y., Yuan, P., Du, P., Deng, L., Wei, Y., Liu, D., Zhong, X., Zhou, J., 2020. A novel halloysite–CeOx nanohybrid for efficient arsenic removal. Appl. Clay Sci. 186, 105450.
Ulrich, R., Martin, R., 1971. Geometrical optics in thin film light guides. Appl. Opt. 10, 2077–2085.
Vergaro, V., Abdullayev, E., Lvov, Y.M., Zeitoun, A., Cingolani, R., Rinaldi, R., Leporatti, S., 2010. Cytocompatibility and uptake of halloysite clay nanotubes. Biomacromolecules 11, 820–826.
Wang, S., Lu, A., Zhang, L., 2016. Recent advances in regenerated cellulose materials. Prog. Polym. Sci. 53, 169–206.
Wu, F., Zheng, J., Li, Z., Liu, M., 2019. Halloysite nanotubes coated 3D printed PLA pattern for guiding human mesenchymal stem cells (hMSCs) orientation. Chem. Eng. J. 359, 672–683.
Xia, D., Quan, P., Piao, H., Piao, H., Sun, S., Yin, Y., Cui, F., 2010. Preparation of stable nitrendipine nanosuspensions using the precipitation–ultrasonication method for enhancement of dissolution and oral bioavailability. Eur. J. Pharm. Sci. 40, 325–334.
Yuan, P., Tan, D., Annabi-Bergaya, F., 2015. Properties and applications of halloysite nanotubes: recent research advances and future prospects. Appl. Clay Sci. 112, 75–93.
Zhu, H., Fang, Z., Preston, C., Li, Y., Hu, L., 2014. Transparent paper: fabrications, properties, and device applications. Energy Environ. Sci. 7, 269–287.